Diffusion of Liquid Polystyrene into a Glassy Poly(phenylene oxide) Matrix. Diffusion Mechanisms and Experimental Verification

J. Pablo Tomba,[†,‡] José. M. Carella,[*,‡,§] David García,[||] and José M. Pastor[||]

Departamento de Ingeniería Química, Departamento de Ingeniería en Materiales, and Instituto de Investigaciones en Ciencia y Tecnología de Materiales (INTEMA) (UNMdP-CONICET), Facultad de Ingeniería, Universidad Nacional de Mar del Plata, Juan B. Justo 4302, (7600) Mar del Plata, República Argentina, and Departamento de Física de la Materia Condensada, Escuela Técnica Superior de Ingenieros Industriales, Universidad de Valladolid, Paseo del Cauce s/n (47011), Valladolid, España

Received March 24, 2000; Revised Manuscript Received November 28, 2000

ABSTRACT: The diffusion of a liquid polymer into a glassy polymer matrix has been studied in a range of temperatures below the glassy matrix glass transition temperature (T_g) and for different diffusion times. The liquid polymer used is low-molecular-weight polystyrene (PS) with a narrow molecular weight distribution, and the glassy matrix is poly(phenylene oxide); the two are miscible at any concentration. A simple physical diffusion model is proposed to correlate and predict diffusion rates, assuming a relatively rapid dissolution of the high-T_g polymer at the liquid−solid interface and a relatively slow diffusion process that produces a thick interphase. The local chemical compositions, local glass transition temperatures, and local PS monomeric friction coefficients change markedly along the diffusion path across the interphase; these changes are well predicted by the diffusion model and have also been experimentally verified. The large changes in local T_g values cause huge changes in the PS monomeric friction factor across the interphase, and this fact explains the asymmetrical local chemical composition profiles experimentally measured for the PS-rich interphase. The results obtained by other authors for the diffusion of liquid polymers and bulky plasticizers into glassy matrixes are analyzed and discussed on the basis of the diffusion model predictions, and it is found that all of them behave following the same pattern as was observed in our experiments. It is concluded that the Case II diffusion mechanism must not be expected for the diffusion of liquid polymers into glassy matrixes, because of the negligible osmotic pressure. Furthermore, all of the analyzed data for diffusion of liquid polymers and bulky plasticizers into glassy matrixes show evidence for relatively rapid dissolution of the glassy matrix at the interface, together with a relatively slow diffusion process across the interphase.

Introduction

Diffusion into amorphous polymer matrixes in the glassy state has received considerable attention in recent years. Many articles have addressed the subject of diffusion of small penetrant molecules (solvent and nonsolvent) over a wide range of concentrations and temperatures.[1−15] Depending on the thermodynamic interaction parameters values, the small-molecule concentration range, and the diffusion temperature, many experiments have been described in which the diffusion does not follow a simple Fick's law with constant diffusion coefficient. Several types of anomalous diffusion behavior have been described and characterized, and some have also been modeled.[1−7,15]

When small molecules penetrate a glassy polymer matrix, diffusion can occur via the Case II mechanism, which is characterized by several specific and well-described conditions.[2−4,6,7,9,10,12] In most Case II diffusion experiments, the glassy polymer is put into contact with an infinite reservoir of small penetrant molecules. In the initial stage, the solvent concentration at the polymer surface increases up to an equilibrium critical concentration ϕ_c. This has been called the "induction period", and a surface swelling kinetics model has been proposed and experimentally verified.[6,9] When a temperature-dependent critical concentration is reached at the surface, a sharp diffusion front is formed that moves into the polymer at a constant velocity V. For sufficiently low activity of the small penetrant molecules outside the solid polymer, experiments indicate that front formation is inhibited.[6,9] When the osmotic pressure of the small molecules reaches the matrix yield stress, the polymer just ahead of the moving front is swollen, and the swelling rate is a function of the osmotic pressure, P_{os}, and the volume fraction of the small penetrant molecules.[10] For most of the studied systems, the penetrant critical concentration is high enough to plasticize the polymer matrix behind the moving front, and in this rubbery phase, the small molecules diffuse very rapidly, with diffusion coefficients higher than 10^{-8} cm^2/s. High diffusion coefficients cause very low (difficult to measure) penetrant concentration gradients behind the moving front. For some glassy polymers with low yield stresses, Case II diffusion starts under high osmotic pressure conditions even when the glass transition temperature of the plasticized glassy polymer at the surface has not decreased to the diffusion temperature;[16] as the swollen outside layer remains in the glassy state, the diffusion coefficients remain lower (in the range of 10^{-12} cm^2/s.), and a small concentration gradient can be observed behind the moving front.[16] The

* Author to whom correspondence should be addressed.
† Departamento de Ingeniería Química, Universidad Nacional de Mar del Plata.
‡ Instituto de Investigaciones en Ciencia y Tecnología de Materiales (INTEMA) (UNMdP-CONICET), Universidad Nacional de Mar del Plata.
§ Departamento de Ingeniería en Materiales, Universidad Nacional de Mar del Plata.
|| Departamento de Física de la Materia Condensada, Universidad de Valladolid.

10.1021/ma000529g CCC: $20.00
Published on Web 02/22/2001

osmotic-pressure-driven deformation ahead of the moving front has been used to derive equations to correctly predict V.[10]

Depending mainly on the front velocity, a Fickian tail is formed ahead of the sharp front. The original model by Thomas and Windle predicts the existence of a Fickian tail ahead of the moving front.[2−4] The conditions that determine the relative importance of the Fickian tail were experimentally verified by assuming that the elongational viscosity ahead of the moving front decreases exponentially with the increase in the penetrant volume fraction.[6]

These aspects of Case II diffusion have been well understood, and quantitative mathematical models that describe the initial stage and the propagation of the sharp front have been developed.[2−4,6,7,14,15] The influences of the diffusion temperatures and the molecular sizes of the small penetrant molecules have been modeled and experimentally verified.[3,4,10,12]

More work has been published dealing with diffusion of larger molecules in the liquid state into polymer matrixes in the glassy state.[17−20]

The diffusion of poly(vinyl methyl ether) (PVME) into a glassy polystyrene (PS) matrix at 24 K below the PS T_g has been studied by neutron reflection (NR) spectroscopy and spectroscopic ellipsometry (SE).[17] The rate of change of the interface penetration depth of PVME into PS is reported to be linear with time, and the experimental techniques are said to reveal some evidence of asymmetric interfacial profiles. It is also mentioned that the linear dependence with time of the interface penetration and that the asymmetric interface profiles can be interpreted in terms of the Case II diffusion process.[17]

The diffusion of liquid PS into a glassy poly(phenylene oxide) (PPO) matrix has been studied using Rutherford backscattering spectrometry (RBS), at temperatures between 39 and 6 K below the matrix T_g.[18] Markedly asymmetric PPO concentration versus depth profiles have been measured at the diffusion interphase, with a low slope at low values of PPO volume fractions and a much greater slope at high values of PPO volume fractions. Values of the Fickian diffusion coefficients D extracted from concentration gradients agree with the Kramer model[21−23] predictions and reveal the importance of considering the local T_g influence on molecular mobilities.[18]

Also, attenuated total reflection Fourier transformed infrared spectroscopy (ATR-FTIR) has been used to study the interdiffusion between PVME and a glassy PS matrix at temperatures of 15 K below and 5 K above the PS matrix T_g.[19] The experimental data obtained for diffusion at 15 K below the PS T_g have been reported to fit a linear combination of Fickian diffusion with constant diffusion coefficient plus a Case II model.

The diffusion of a plasticizer [resorcinol bis(diphenyl phosphate), RDP] into an engineering amorphous thermoplastic (ULTEM) has been studied using the RBS technique in a temperature range between 95 and 55 K below the glassy ULTEM T_g.[20] The RDP volume fraction versus diffusion distance profiles in the glassy polymer were found to be essentially step functions with sharp diffusion fronts. The experiments were performed under conditions of a limited plasticizer supply, and therefore, the plasticizer concentration at the outer layer decreased with diffusion time. The diffusion was observed to stop when the T_g of the plasticized outer layer decreased to the vicinity of the diffusion temperature. The advancing front velocities were found to change markedly with the plasticizer volume fraction at the plasticized outer layer, but only qualitative explanations are given in terms of Deborah number De.[1]

Table 1. Molecular Weight and T_g Characterization Data for Pure Samples

sample	$\bar{M}_n$ (g/mol)	$\bar{M}_w$ (g/mol)	T_g (K)
PPO	15500	31000	485
PS850	710	850	256
PS740	700	740	268

At this point we must make clear the difference used to establish between the terms small molecules and large molecules. We will define small molecules as those that, in contact with the glassy polymer matrix at concentrations near the equilibrium critical concentration ϕ_c, will produce osmotic pressures in the range of the glassy matrix yield stress (these being temperature-dependent phenomena). On the other hand, we will define large molecules as those that, under the above-mentioned conditions, will produce osmotic pressures that are far below the glassy matrix yield stress. The osmotic pressure is known to depend inversely on the penetrant molecular volume,[6] and this is the basis used to distinguish between small and large molecules.

The diffusion processes for small molecules into glassy polymer matrixes have been thoroughly described in terms of quantitative physical models, and almost every aspect of the influences of different variables has been clarified. For large molecules, on the other hand, most of the existing experimental data have not been quantitatively interpreted on the basis of a generalized, solid theoretical frame. This is the topic in which we are interested.

For this work, the diffusion of liquid large molecules (PS) into a glassy PPO matrix has been experimentally studied in a temperature range between 90 and 15 K below the glassy matrix T_g and for a wide range of diffusion times. The PS volume fraction versus penetration depth profiles have been measured by a direct technique (confocal Raman microspectroscopy). The experimental results have been interpreted in terms of an already-established diffusion model that takes into account the local molecular weights distributions, thermodynamic interactions, monomeric friction coefficients for all chemical species, and glass transition temperatures.[21−25] The experimental results for the diffusion of large molecules that have been published by other authors and were previously mentioned are also analyzed on the same theoretical basis.

Experimental Section

Two types of miscible polymers were used for the experiments: polystyrene (PS) and poly(phenylene oxide) (PPO). Two anionically polymerized polystyrene samples (PS850 and PS740) were purchased from Polymer Source (Dorval, Canada); the maker labeled these samples as P446-St and P1779-St. Molecular weight characterization details for all of the samples used were provided by the makers and can be found in Table 1. The only PPO sample used was provided by General Electric. All samples were exhaustively dried under vacuum before use, to remove any traces of solvent or moisture present, because small amounts of solvents can markedly change the T_g.

Homogeneous blends were prepared by weighing the polymers in the desired proportions, dissolving the solids in benzene at room temperature [about 10% (w/v) solutions], and freeze-drying the necessary amounts of the solutions.

Table 2. Composition (wt %) and T_g Characterization Data for the Blends Used for Experiment Types A−D

exp type		PPO	PS850	PS740	T_g (K)	diffusion temp (K)
A	thin	40	60	−	312	403
	thick	80	20	−	413	
B	thin	20	−	80	285	393
	thick	90	−	10	443	
C	thin	20	−	80	285	393
	thick	95	−	5	463	
D	thin	5	−	95	277	373
	thick	95	−	5	463	

Glass transition temperatures for pure polymers and homogeneous blends were determined by differential scanning calorimetry (DSC), using DuPont 990-DSC and Shimadzu DSC-50 instruments. Reported T_g values were always calculated as the onset of the thermal transition. A set of six PS−PPO blends of known compositions were used to obtain T_g versus composition data for each PS sample used.

Slender composite plates were prepared as described elsewhere.[26] For each composite plate, a thick layer (about 900 μm thick) was prepared by vacuum molding a blend with one of the high-T_g compositions specified in Table 2, at temperatures at least 20 K above the blend T_g. Thick layers were made from a blend of PPO and a small quantity of PS (as shown in Table 2) to lower the PPO T_g and overcome the difficulties of molding pure PPO. A thinner layer (typically between 10 and 80 μm thick) of the corresponding low-T_g PS blend was then vacuum molded on top of the thick layer, at temperatures conveniently chosen to be below the thick-layer T_g, to minimize diffusion at this stage. The thin-layer thickness is included in the figures, which show PS volume fraction versus diffusion coordinate data (calculated and experimental), as h_i. At least four samples were used for each type of experiment detailed in Table 2, with different starting thin-layer thicknesses and diffusion times. Experiments A−D were designed to explore a range as wide as possible in the difference between the diffusion temperature and the glass transition temperature of the PPO-rich layer.

The diffusion between layers of the composite plates was promoted by elevating the temperature in a controlled vacuum oven for specified periods of time. Temperatures and times for each diffusion experiment are also shown in the corresponding figures.

Local Raman spectra for pure PPO, pure PS and blends were measured at room temperature on a Raman DILOR LabRam confocal microspectrometer , using a 16-mW He−Ne laser beam. The slit opening used was 500 μm, with a pinhole opening of 100 μm and a holographic grating of 1800 lines/mm, which allows for the acquisition of data in a frequency range between 500 and 1500 cm^{-1}. The characteristic Raman bands used for calculations are located in this frequency range. Local spectra (for small regions of about 2-μm nominal diameter) were measured along the diffusion coordinate, with the laser beam aligned in a direction parallel to the diffusion coordinate. Many spectra were acquired, with the laser beam focused at different depths along the diffusion path, as described in an earlier work.[27] Local chemical compositions were calculated from the acquired local Raman spectra using a linear decomposition method.[28] Some selected spectra were also processed using a conventional deconvolution and curve-fitting procedure; both methods give essentially the same results, in terms of experimental error, but the linear decomposition procedure gives more consistent results.[30]

Confocal Raman microspectrometers show a characteristic bell-shaped spatial resolution curve in any direction parallel to the laser beam axis. Whereas the nominal resolution for the systems used is 2 μm (fwhm), the tails of the bell-shaped curve reach distances on the order of tenths of micrometers in the depth direction.[29] The characteristic resolution curve is routinely measured by using an optically flat air−silicon interface, and for this study also a flat plate made out of a 50/50 (w/w) PS−PPO blend was used, and similar resolution curves were obtained. The calculated PS volume fraction versus diffusion distance profiles were convoluted with the measured spatial resolution curve. Details of the methods used can be found elsewhere.[30]

Physical Diffusion Model Used

As the osmotic pressure generated by the PS in contact with the PPO glassy surface is extremely low, it is assumed that the interface thickness and chemical composition versus depth profiles are kinetically controlled by a relatively rapid dissolution of PPO-rich layer into the PS-rich layer. The rate of penetration of PS into the PPO-rich glassy matrix is negligible.

On the above-mentioned basis, interdiffusion processes between PS and PPO, each one with a given distribution of degrees of polymerization ($l_1^{PS} \le l^{PS} \le l_2^{PS}$) and ($l_1^{PPO} \le l^{PPO} \le l_2^{PPO}$) can be described by the following set of diffusion equations:[21,24,25]

$$\frac{\partial \Phi_l^{PS}}{\partial t} = \vec{\nabla}(\Lambda_l^{PS} \cdot \nabla \mu_l^{PS}) + \vec{\nabla}(\Phi_l^{PS} \cdot \vec{J}_v) \qquad (1A)$$

$$\frac{\partial \Phi_l^{PPO}}{\partial t} = \vec{\nabla}(\Lambda_l^{PPO} \cdot \nabla \mu_l^{PPO}) + \vec{\nabla}(\Phi_l^{PPO} \cdot \vec{J}_v) \qquad (1B)$$

In eqs 1, Φ_l^i is the concentration (volume fraction) of polymer i with polymerization degree l, and μ^i and Λ^i are the chemical potential and diffusivity (Onsager coefficients) of species i, respectively.[21] The bulk flow $\vec{J}_v$ is defined by

$$\vec{J}_v = \vec{J}^{PS} + \vec{J}^{PPO} \qquad (2)$$

where

$$\vec{J}^i = -\sum_{l=l_1^i}^{l_2^i} \Lambda_l^i \cdot \vec{\nabla} \mu_l^i \qquad (3)$$

The system of equations 1 is required to satisfy the following restriction at every point along the diffusion coordinate:

$$\sum_l \Phi_l^{PS} + \sum_l \Phi_l^{PPO} = 1 \qquad (4)$$

This simple mass conservation equation is equivalent, at the liquid PS−glassy PPO interface, to a dissolution velocity much faster than the diffusion process, as it provides PPO to the liquid layer without limits other than those established by the diffusion equations. Consistently, the nonflux or Newmann boundary conditions are used at the outer surfaces of the sample.

The chemical potentials are described by the Flory−Huggins theory for polydisperse systems as

$$\mu_l^{PS} = kT\left[\frac{1}{l} + \frac{1}{l}\ln(\Phi_l^{PS}) - \left(\frac{\Phi^{PS}}{\bar{x}^{PS}} + \frac{\Phi^{PPO}}{\bar{x}^{PPO}}\right) + \chi(\Phi^{PPO})^2\right] \qquad (5)$$

where the total concentration of polymer i is defined as

$$\Phi^i = \sum_i \Phi_l^i \qquad (6)$$

A similar equation is used for the chemical potentials of all PPO molecular weights. Here, $\bar{x}^{PS}$ and $\bar{x}^{PPO}$ are

the number-average degrees of polymerization for PS and PPO, respectively.

The expression for the binary diffusion coefficient, assuming monodisperse components, becomes

$$D = kT(\Phi^{PPO}\Lambda^{PS} + \Phi^{PS}\Lambda^{PPO})\left[\frac{\Phi^{PS}}{l^{PPO}} + \frac{\Phi^{PPO}}{l^{PS}} - 2\chi\Phi^{PS}\Phi^{PPO}\right] \quad (6')$$

In the range of blend composition selected for this work, the PS samples used have all average molecular weights smaller than the entanglement molecular weights of the blends.[31] For this reason Rouse dynamics is assumed for all of the PS species. In this case, the Onsager coefficient for PS becomes[21,24]

$$\Lambda_l^{PS} = \frac{1}{\zeta_0^{PS}}\Phi_l^{PS} \quad (7)$$

where ζ_0^{PS} is the monomeric friction factor for the PS species.

The monomeric friction coefficients for the PS−PPO blends, measured at a constant temperature increment over the value of $T_{g,blend}$, are markedly dependent on blend composition. Experimental values of the monomeric friction factors for PS and PPO as functions of blend composition were taken from Figure 4 of ref 23 and were corrected to different temperatures using a standard WLF equation.[32]

For the whole blend composition range used, the PS monomeric friction factor is at least 1 order of magnitude smaller than the PPO monomeric friction factor. In addition, the average molecular weights for PPO are much higher than those for PS. Therefore, the low-molecular-weight PS species used for this work are the fast-diffusing species that control the diffusion process.

The WLF equation used to model the strong dependence of friction factors on temperature and on the local T_g ($T_{g,blend}$) is[32]

$$\log\frac{\zeta_0(T_{ref})}{\zeta_0(T)} = \frac{-12.0(T - T_{ref})}{50.0 + T - T_{ref}} \quad (8)$$

where $T_{ref} = T_{g,blend} + 3$ K.

Along the diffusion path, the chemical compositions and molecular weight distributions change between two very different ends. This fact causes the local physical properties to change markedly, and therefore, the calculation scheme must take this fact into account. All of the above-mentioned local properties are calculated for each diffusion step. The environmental dependence is established through the local T_g, which is a function of the local composition. A low-degree polynomial was used to fit the T_g versus chemical composition experimental data.

For many polymer pairs, the Flory−Huggins thermodynamic interaction parameter (χ) has been experimentally found to depend on temperature, chemical composition, molecular weights, and the presence of isotopes.[22] Because of the lack of more adequate experimental data, for the simulations performed for this work, χ was supposed to be independent of local blends composition and to depend only on temperature. The data used were reported for the dPS−PPO system in ref 22.

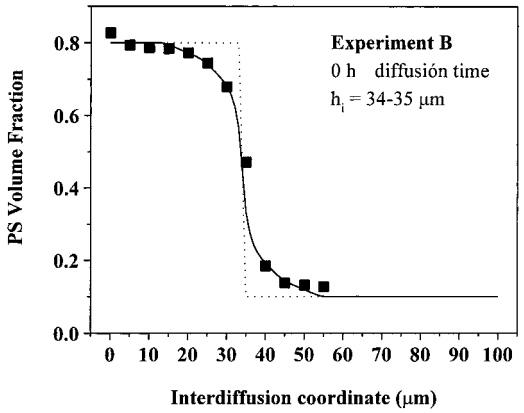

Figure 1. Local PS volume fractions for a sample used for a type B experiment before difussion. The dotted line represents data obtained from micrometer and weighing measurements. The solid line represents data from the dotted line, convoluted with the experimentally measured confocal Raman resolution curve. Solid squares represent values calculated from Raman experimental measurements.

A finite-differences scheme has been used to solve the system of equations 1, as detailed in ref 24.

Results and Discussion

Liquid PS Diffusion into Glassy PPO Matrix. Figure 1 shows, as solid squares, data calculated from the Raman experimental measurements for a sample used for a type B experiment. Local PS volume fraction values are plotted versus diffusion coordinate. This sample has not undergone any thermal treatment to promote diffusion, and therefore, we expect to find a sharply defined interphase composition profile with only minor rugosities, as mentioned before by other authors.[19] The thick layer of this sample was molded at 480 K (40 K above the thick-layer T_g), and then the thin layer was molded on top of this at 310 K (25 K above the thin-layer T_g and 130 K below the thick-layer T_g) for about 15 min. Under these conditions, we can safely assume that the Fickian diffusion coefficient for the PS species in the glassy thick layer is lower than 10^{-20} cm^2/s.[10] Any calculation will show that the diffusion caused by this sample preparation will not be observed on the Figure 1 abscissa scale. Included in Figure 1 as a thin dotted line is the composition profile calculated from micrometer and weighing measurements, which takes the shape of a step function. The values of the step function were convoluted at each point with the corresponding confocal Raman spatial resolution curve, to calculate the values to be expected from the calculations based on confocal Raman experimental measurements, and the results are shown as a thin solid line.[30] Because the agreement between the experimentally measured and expected values is so good, we are convinced that the two observed tails (ahead and behind of the sharp interface) are completely fictitious, caused by the instrumental confocal Raman microspectroscopy spatial resolution, as mentioned in the Experimental Section.

It must be pointed out that the percent error caused by the confocal Raman microspectrometer spatial resolution will not be the same for high or low slopes in the chemical composition (PS volume fraction) versus depth profiles. As the bell-shaped curve is extended along the depth (or diffusion coordinate) direction, lower slopes will be much less affected by the enlargement of the region over which the Raman signal is effectively averaged, as shown in Figure 1.

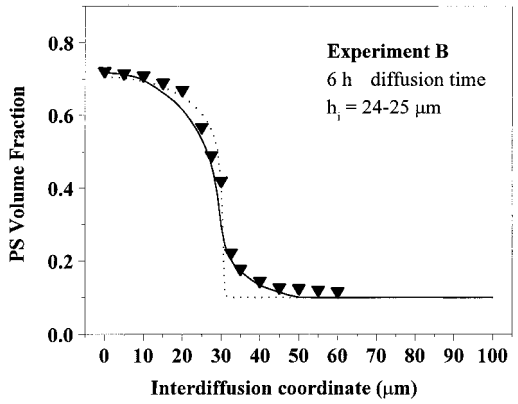

Figure 2. Local PS volume fractions for a sample used for a type B experiment, after 6 h of diffusion. The dotted line represents data obtained from model predictions. The solid line represents data from the dotted line, convoluted with the experimentally measured confocal Raman depth resolution curve. Solid triangles represent values calculated from Raman experimental measurements.

Figure 2 shows, as solid triangles, data calculated from Raman experimental measurements, for another sample used for a type B experiment. Local PS volume fraction values are also plotted versus diffusion coordinate. This sample was kept at 393 K for 6 h in a vacuum oven to promote diffusion. The diffusion temperature is located 50 K below the glassy matrix T_g. The thin dotted line shows the expected chemical composition versus depth profile, calculated by the above-mentioned physical diffusion model. The thin solid line represents the calculated values shown by the dotted line, convoluted by the instrumental spatial resolution curve. The agreement between the thin solid line and the solid triangles is excellent for depths of up to 30 μm, and a fictitious tail appears between 30 and 50 μm, as expected from the above discussion. The interface between the original PS-rich thin layer and the glassy matrix for this sample was originally located at 24.5 μm, and after diffusion, it had advanced up to 31.5 μm. The calculation correctly predicts the experimentally observed chemical composition profile, once the fictitious instrumental tail is disregarded. As expected from the physical diffusion model, the highest slope, associated with a higher T_g, is located next to the glassy matrix, and a gradually decreasing slope shows the influence of the rapidly changing T_g profile along the diffusion path. For experiments conducted 1 K below the glassy matrix T_g value in earlier work, it has been shown that when the local T_g changes by about 80 K along the diffusion path, the PS monomeric friction coefficient changes by about 7 orders of magnitude,[33] thus justifying the chemical composition profile shape shown in Figure 2. Similar agreement between convoluted model calculations and experimental Raman data was obtained for all of the diffusion experiments of types A−C. Anomalies were found for experiments of type D, which will be discussed later.

Figures 3−5 show experimental Raman data for all experiments of types A−C, for which the experimental details can be found in Table 2. (For experiments A−D, the difference between the glassy matrix T_g and the diffusion temperature has been systematically increased for a specific purpose.) In Figure 4, convoluted model calculation results are also shown as solid lines; this type of information is not included in Figures 3 and 5 for the sake of clarity. The physical model used accurately predicts every detail of the time evolution of the chemical composition profiles for all of these experiments. Both the depth evolution with time of the highest slope next to the glassy matrix and the decrease in the PS concentration at the samples' outer surfaces are clear

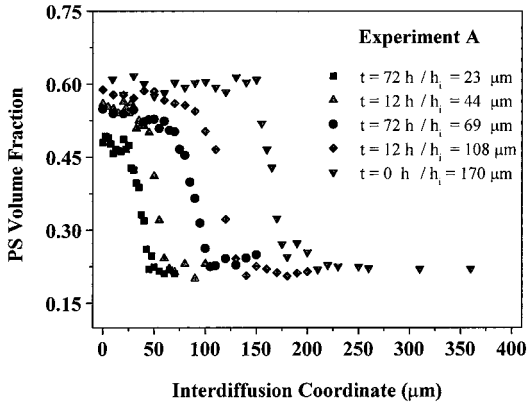

Figure 3. Local PS volume fractions calculated from Raman measurements for all of the type A experiments. The diffusion temperature can be read from Table 2. The diffusion time for each experiment is shown. The thin-layer thickness before diffusion is included and labeled h_i. It must be noted that not all of the samples had the same starting thin-layer thickness.

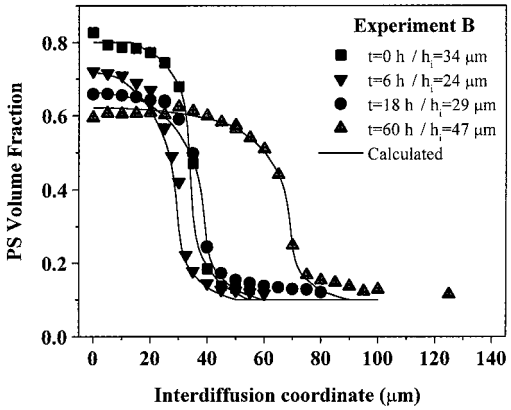

Figure 4. Local PS volume fractions calculated from Raman measurements for all of the type B experiments. The diffusion temperature can be read from Table 2. The diffusion time for each experiment is shown. The thin-layer thickness before diffusion is included and labeled h_i. The solid lines show model predictions for each experiment, convoluted with the Raman experimental depth resolution curve.

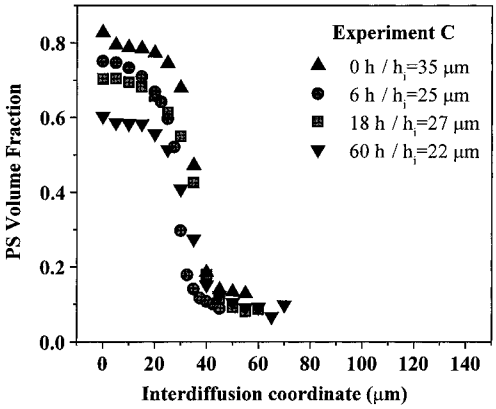

Figure 5. Local PS volume fractions calculated from Raman measurements for all of the type C experiments. The diffusion temperature can be read from Table 2. The diffusion time for each experiment is shown. The thin-layer thickness before diffusion is included and labeled h_i.

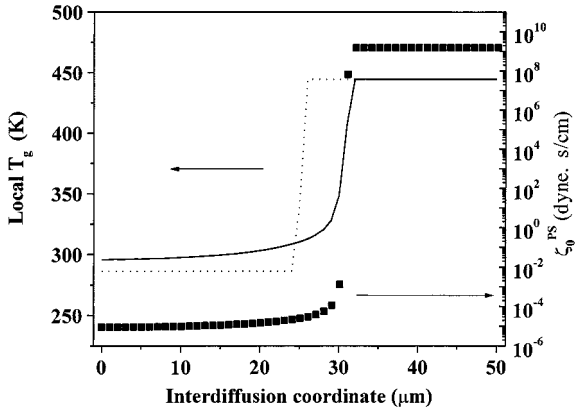

Figure 6. Local T_g values for a type B experiment, before (dotted line) and after (solid line) diffusion. Solid squares show local monomeric friction coefficient values. Details are explained in the text.

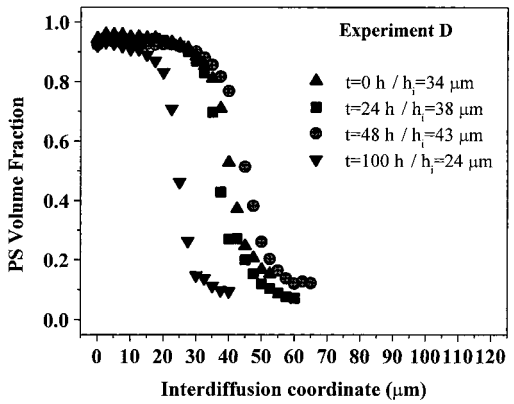

Figure 7. Local PS volume fractions calculated from Raman measurements for all of the type D experiments. The diffusion temperature is 373 K. The diffusion time for each experiment is shown. The thin-layer thickness before diffusion is included and labeled h_i.

evidence in support of the proposed physical diffusion model.

The penetration of the liquid PS into the glassy matrix is negligible, as is expected on the basis of the extremely low diffusion coefficient mentioned above, and therefore, no Fickian tail is expected ahead of the moving interface. The liquid PS dissolves PPO relatively rapidly. This is demonstrated by the fact that the physical diffusion model used for calculations and simulations in this work has also been used with success for the study of liquid−liquid diffusion experiments using the same polymer pair at temperatures above the PPO-rich-layer T_g.[22,24,25] The diffusion process is characterized by the transport of PS from the original PS-rich thin layer into layers that are richer in PPO, and the PPO transport is always realized toward layers with lower local T_g values. The whole dynamics for the faster-diffusing species (PS) is Rouse-type, as shown in earlier works.[24,25,33] For the entire chemical composition range used, the monomeric friction factor for the PS species follows the WLF dependence on temperature, through the parameter $(T - T_g)$.[33]

Figure 6 shows local T_g value versus diffusion coordinate profiles for the same type B experiment shown in Figure 2. A dotted line corresponds to the original sample (experimental results) before diffusion was promoted. A solid line shows the calculated T_g profile for the same sample after diffusion (6 h at 393 K). The T_g versus diffusion distance curve is calculated from the composition profile (Figure 2) predicted by the diffusion model and the experimental T_g versus chemical composition experimental data. This type of calculation has been experimentally verified in earlier works.[24,25] As expected, the highest slope in T_g corresponds to the highest slope in chemical composition, which explains the abrupt change in PS monomeric friction coefficient, shown as solid squares, calculated as mentioned before. The markedly asymmetric monomeric friction coefficient profile explains the also asymmetric PS concentration profile. This is a general pattern, which we expect to arise for any process involving diffusion of a liquid polymer into a non-crosslinked, glassy polymer matrix. The values displayed for the PS monomeric friction coefficient inside the glassy matrix have not been experimentally measured but have been calculated from the experimentally measured values for the liquid state; the extremely steep WLF dependence makes these calculations very uncertain, but the trend is correct.

Experiments B and C were designed to test diffusion of the same liquid PS into matrixes with different T_g values, for a specific purpose that will be discussed later. The model calculations for these experiments also agree with the experimental results, well within the experimental error limits.

Experimental results calculated from Raman measurements for samples used in type D experiments are shown in Figure 7. The local PS volume fraction versus diffusion distance profiles follow the same qualitative behavior as for experiments A−C, but the convoluted calculation results predict faster diffusion, as shown in Figure 8A for a sample used for a type D experiment, after 24 h of diffusion at 373 K. There is no reason to expect a change in the diffusion physics for the type D experiments, and the observed qualitative behavior seems to confirm this expectation. Looking for a reason for this discrepancy, we discarded changes in the WLF parameters, which have given excellent results for the other experiments. A temperature-dependent parameter to be analyzed is the Flory−Huggins thermodynamic interaction parameter χ. It is well-known that several miscible polymer blends display not only lower critical solution temperature (LCST) behavior but also phase separation at low temperatures. The simultaneous occurrence of a LCST as well as an upper critical solution temperature (UCST) has been described as a rather general phenomenon.[34] Several polymer pairs that display simultaneous LCST and UCST behavior are also cited in ref 34. It has also been pointed out that, in most of the cases, the UCST is located below the glass transition temperature and becomes experimentally inaccessible. This might well be the reason for the observed slowing for the diffusion experiments of type D.

Other authors[22] have precisely measured χ for this dPS−PPO system over a range of temperatures between 454 and 588 K. Results taken from ref 22 (Figure 9) have been used for calculations for many diffusion experiments conducted between 450 and 483 K with excellent results.[24,25] A linear extrapolation of the results shown in Figure 9 of ref 22 has been used for calculations for diffusion experiments A−C, run at temperatures lower than 453 K, and no meaningful discrepancies were observed for the experiments run at temperatures down to 393 K.

We have examined carefully the influence of the χ parameter on the PS diffusion rates in the region close

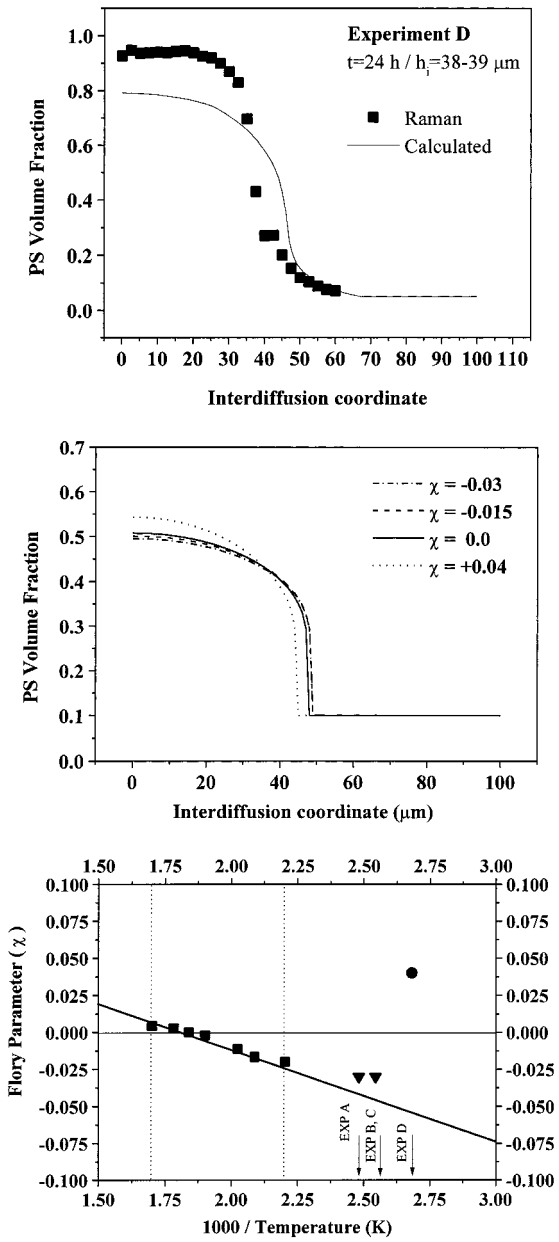

Figure 8. (A) Local PS volume fractions for a type D experiment. Values calculated from Raman experimental measurements are shown as solid squares. The solid line shows the convoluted model prediction. The diffusion temperature is 373 K. The diffusion time is 24 h. The thin-layer thickness before diffusion is included and labeled h_i. (B) Local PS volume fractions for a type B experiment. The lines show the expected composition profiles, based on simulations performed using the χ values shown in the legends. (C) Flory interaction parameter χ for the PPO−PS system versus inverse temperature. The solid squares show experimental data taken from ref 22 (vertical dotted lines show the experimental temperature range used). The solid triangles show χ values used for simulations of experiments A−C. The arrows show the diffusion temperatures used for experiments A−D.

to the diffusion front. From the mathematical formulation of the diffusion model proposed stems the following points:

(a) For the low-polymerization-degree PS used for these experiments, the influence of the entropic term on the thermodynamic factor arising from the chemical potential gradient is more important than the enthalpic term (eqs 3 and 6′); this makes the diffusion rates quite a bit less sensitive to the χ values.

(b) From the form of eq 6′, we can appreciate that the influence of χ is highest at intermediate compositions (Φ^{PS} close to 0.5). Also, the influence of χ on Φ^{PS} closer to 0 becomes negligible.

(c) These observations suggest that the PS will dissolve all necessary amounts of PPO at the interface (where the value of the thermodynamic factor is at a maximum) driven by the strong influence of the enthropic term. The PPO transport away from the interface will be controlled by the diffusion process at higher Φ^{PS} values, where the χ influence becomes somewhat more important.

(d) Points a−c also indicate that, for the proposed model in its present form, the assumption of χ being independent of chemical composition is of minor importance.

(e) A quick calculation done for $\Phi^{PS} = 0.5$ shows that the enthalpic term accounts for 28% of the thermodynamic factor if $\chi = -0.03$. The same enthalpic term accounts for 66% of the thermodynamic factor if $\chi = 0.04$. These numbers suggest that small differences for negative values of χ will make smaller differences in the thermodynamic factor values than small differences for positive values of χ.

Figure 8B shows diffusion simulations performed for experiment B. For this purpose, several χ values were used, ranging from −0.030 to 0.040. First, it should be noted that the differences between the simulations performed using χ values between 0 and −0.030 can hardly be distinguished from experimental error. Second, a positive value of $\chi = 0.040$ makes a large difference, which can be experimentally verified. Figure 8C shows χ data taken from Figure 9 of ref 22, as solid squares. Solid triangles show χ values used for simulations of experiments A−C. A solid circle shows $\chi = 0.04$. Using $\chi = 0.04$, the experimental data for experiment D shown in Figure 8A can be exactly reproduced. Also, the experimental data for experiments A−C can be reproduced within experimental error by using a value for χ less favorable than −0.03, as shown in Figure 8B. Using χ values closer to 0 than −0.03 in Figure 8C, a smooth curvature can fit the experimental data from ref 22 and the χ values used for this work and suggested in this section ($-0.03 < \chi < 0$ for experiments A−C, and $\chi = 0.04$ for experiment D).

On the basis of the above observations, it seems possible that the χ value for this PPO−PS system takes a small positive value at the temperatures used for experiment D. Further experiments are being conducted to clarify this point.

Comparison with Other Similar Diffusion Experiments. A set of diffusion experiments mentioned before, on the diffusion of a plasticizer [resorcinol bis(diphenyl phosphate) (RDP)] into a glassy matrix made of an engineering amorphous thermoplastic (ULTEM),[20] shows remarkable similarity with our PS−PPO diffusion experiments. First, the diffusion was studied in the temperature range between 95 and 55 K below the glassy matrix T_g. Second, the plasticizer is completely soluble in the matrix polymer. Third, the molar volume of the plasticizer is smaller than but similar to the molar volume of the PS used in our experiments, and this fact qualifies the plasticizer as a large molecule, as described before. Fourth, both the RPD−ULTEM and the PS−PPO diffusion experiments analyzed in this work also fulfill the condition of limited supply.

All of the main characteristics observed in the RDP−ULTEM diffusion experiments have also appeared in our PS−PPO diffusion experiments. (a) The volume fraction versus depth profiles for RDP and PS are essentially step functions, with sharp diffusion fronts. (b) With the low-T_g species (PS or RDP) in limited supply, its concentration at the outer layer decreased with diffusion time. (c) For the RDP experiments, the diffusion was observed to stop when the plasticized outer-layer T_g decreased to the vicinity of the diffusion temperature, and the same behavior is predicted by the diffusion model used for calculations in our PS−PPO system. (d) The advancing front velocities for both sets of experiments were found to decrease markedly with the decrease in the low-T_g species concentration at the plasticized outer layer, and this decrease is correctly predicted by the diffusion model used for calculations in our PS−PPO system. (e) The experimental measurement technique used for the RDP−ULTEM system (RBS) is also said to show a bell-shaped depth resolution curve, which causes a fictitious tail on the order of 50 nm (fwhm) to appear ahead of the moving front.

Because of the above-detailed similarities, we understand that the physical principles that govern the diffusion process for the above-mentioned RDP−ULTEM experiments are the same as those governing the PS−PPO system under the experimental conditions used for our experiments. For this reason, we believe that the same physical diffusion model can be used to predict all of the main characteristics of these diffusion processes.

As all of the experimentally measured PS volume fraction versus diffusion coordinate profiles (for different diffusion times and conditions) (Figures 3−5) coincide precisely with the simulation results based on the physical model used, in what follows, we use simulation results to predict the needed results that have not been experimentally measured. Therefore, we have used the diffusion model to predict the behavior of the PS−PPO system in diffusion experiments conducted under conditions similar to the conditions used for the RDP−ULTEM system experiments; the simulations have been performed at temperatures located between 75 and 95 K below the glassy matrix T_g, under conditions of limited PS supply. Figures 9−12 show the simulation results, adequately displayed to compare with the RDP−ULTEM published diffusion results analysis.[20]

Figure 9 shows the time evolution of the PS volume fraction at the PS-rich layer outer surface, for C-type PS−PPO diffusion experiments as lines. The basic information to be extracted is that the model also predicts that the diffusion slows with time and completely stops once the PS-rich-layer T_g has decreased to the diffusion temperature, because of the WLF dependence of the monomeric friction coefficient for PS. Open squares and triangles show equivalent data taken from the RDP−ULTEM experiments described in ref 20 (Figure 13) for comparison purposes. The same trends can be observed for both sets of experiments: for short diffusion times, the RDP and PS volume fractions decrease rapidly, and the rate of change decreases continuously with time. The difference in horizontal scales is due to the differences in monomeric friction coefficients and mobilities between the two sets of experiments (RDP−ULTEM and PS−PPO); the vertical shifts are due to the slightly different starting experimental conditions used for each set of experiments.

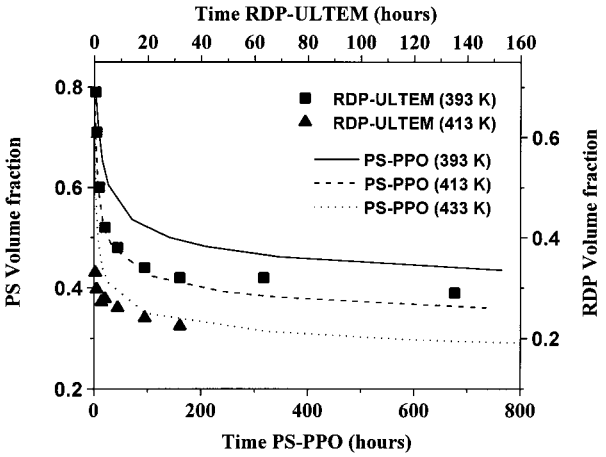

Figure 9. Time evolution of the PS volume fraction at the PS-rich layer outer surface for PS−PPO type C diffusion experiments, shown as solid lines. Simulated results for other diffusion temperatures are shown as dashed and dotted lines. Data for the RDP-rich outer surface have been taken from ref 20 (Figures 9 and 13) and are shown as symbols. Details are explained in the text.

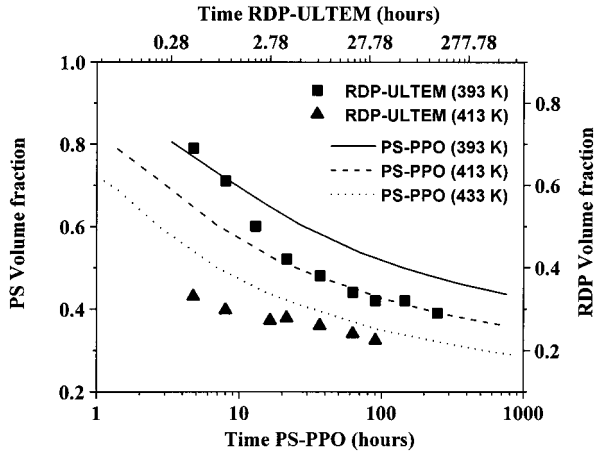

Figure 10. Data from Figure 9 shown with a logarithmic scale for time, for comparison with the results published in ref 20. Details are explained in the text.

Scatter observed for the RDP−ULTEM diffusion data is believed to be caused mainly by RDP losses caused by the small but meaningful vapor pressure for the RDP at the diffusion temperature.[20] Larger errors are expected for higher diffusion temperatures. The PS−PPO system does not show this inconvenient feature.

Figure 10 shows the same type of information as Figure 9, plotted as a function of the logarithm of time. Data for RDP diffusion into ULTEM, taken from Figure 13 of ref 20, are also shown as solid symbols for comparison. The purpose of this plot is to show that the model predicts, for these limited-supply experiments, a smooth but important change of slope at any diffusion temperature, caused simply by the dependence of the model physical parameters on the local chemical compositions. The thermodynamic interaction parameter is assumed to depend only on temperature and, therefore, to have no influence on the slopes changes. The temperature difference ($T - T_g$) depends on the elapsed diffusion time, because of the changes in the compositions of the plastized layers; for the two systems, T_g changes smoothly with chemical composition, following similar Fox-type equations, and its influences on the curvature of the simulations and experimental data

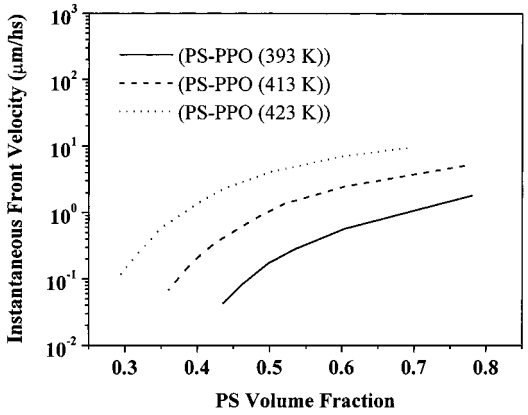

Figure 11. Simulated results for the true instantaneous velocity of the diffusion front for type C PS−PPO diffusion experiments plotted as a function of PS volume fraction at the plasticized outer layer. Details are explained in the text.

shown in Figure 10 are expected to be similar for the two systems (RDP−ULTEM and PS−PPO). The monomeric friction factor depends on the temperature difference $T - T_g$ and the chemical composition. For the PS−PPO system, the values for ζ_0^{PS} at constant $T - T_g$, taken from ref 23, change by a factor of about 10, whereas Φ^{PS} changes from 0.9 to 0.1; this change is responsible for most of the curvature observed in the simulations shown in Figure 10. We have no experimental data for the ζ_0^{RDP} dependence on Φ^{RDP} at constant $T - T_g$, but we understand that ζ_0^{RDP} can easily change by a factor on the order of 10 or higher, while Φ^{RDP} is changed from 0.8 to 0.3. We have selected the data for experiments conducted at 393 K for the RDP−ULTEM system and performed some simulations for the diffusion experiments. Assuming that ζ_0^{RDP} changes smoothly by a factor of 50, the simulation results show the same curvature as do the data from the diffusion experiments conducted at 393 K on the RDP−ULTEM system. We think that such a change in ζ_0^{RDP} can easily be expected in the experimental Φ^{RDP} range used in ref 20. Experimental data reported for ζ_0^{PS} as a function of Φ^{PS} for the diffusion of PS into PS−PVME mixtures shows changes by a factor of at least 100.[35]

In Figure 13 of ref 20, the authors drew two straight lines to fit data obtained from diffusion experiments conducted at 393 K and claimed that the different slopes at short and long diffusion times correspond to a change in diffusion mechanism (Case II at short times and anomalous diffusion at long times). The change on the slope for the curve corresponding to diffusion experiments conducted at 493 K can be due to large changes in the monomeric friction factor; the curves corresponding to diffusion experiments conducted at higher temperatures show minor changes of slope, which can be expected because these experiments cover a much narrower range of Φ^{RDP} values. No change of diffusion mechanism seems to be needed to reproduce the RPD−ULTEM results for the whole diffusion temperature range used.

Figure 11 shows simulated results for the true instantaneous velocity for the diffusion front for type C PS−PPO diffusion experiments plotted as a function of the PS volume fraction at the plasticized outer layer. As predicted by the model physics, the front displacement velocity for any of these experiments decreases when the PS concentration at the outer layer decreases,

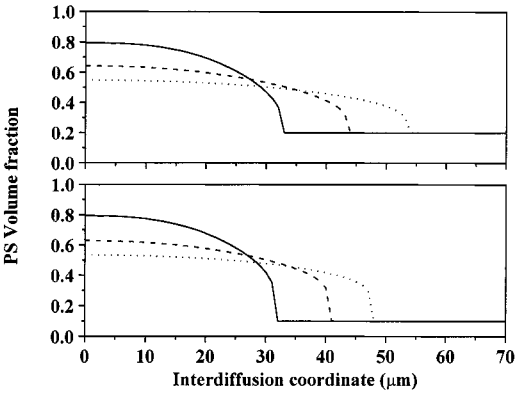

Figure 12. Simulated results for diffusion experiments of the same PS into two matrixes with different T_g values. Local PS volume fraction values for simulated diffusion experiments into the lower-T_g matrix, for several diffusion times, are shown in the upper part, and the equivalent data for experiments simulated for the higher-T_g matrix are shown in the lower part. The horizontal scale is the same for both sets of data. Details are explained in the text.

simply because of the increase in the local T_g value at every point of the plasticized outer layer. There is a clearly observable change in slope for the curve corresponding to every diffusion temperature. The simulated data clearly resemble the experimental data plotted in Figure 14 of ref 20, giving support to our claim that there is no change in diffusion mechanism associated with the change in the plasticized layer composition.

As mentioned before, experiments B and C were designed to test diffusion of the same liquid PS into glassy matrixes with different T_g values for a specific purpose that now becomes clear. Figure 12 shows simulated results for diffusion of the same PS into two different matrixes with matrix T_g values that are about 30 K apart. Simulated PS local volume fraction values for diffusion experiments into the glassy matrix with the lower T_g value for several diffusion times are shown in the upper part. The equivalent data for diffusion experiments into the glassy matrix with the higher T_g value are shown in the lower part. We observe clearly that the diffusion front speed for the set of experiments carried out with the lower-T_g matrix is higher than for the experiments carried out with the higher-T_g matrix. This result is simply due to the fact that the local T_g at the glassy matrix interface is lower for experiments shown in the upper part of Figure 12, and therefore, the local T_g at any point of the diffusion interphase is lower. The same type of results have been observed for the already-mentioned RDP−ULTEM diffusion experiments (Figure 12 of ref 20), when diffusion of RDP into a pure ULTEM matrix are compared with diffusion of RDP into an ULTEM matrix previously plasticized with 8% RDP. These results have not been satisfactorily explained.

At this time, we must point out that diffusion experiments for liquid PS into glassy PPO matrixes, as well as for RDP into glassy ULTEM, proceed by the same mechanism: (a) the glassy matrix is dissolved relatively rapidly at the interface, and (b) the diffusion process is controlled by the local T_g. There is no evidence for Case II diffusion for any of these experiments, and further support for this claim is given by the results obtained for diffusion of RDP into ULTEM under an externally applied tension, where no increase in diffusion front speed is observed. The diffusing species used for these

systems do not seem to generate enough osmotic pressure to reach the glassy matrix yield stress and produce a Case II diffusion mechanism.

Other Diffusion Experiments with Larger Molecules in the Liquid State. The diffusion of poly(vinyl methyl ether) (PVME) into a glassy polystyrene (PS) matrix at 24 K below the PS T_g studied by neutron reflection (NR) and spectroscopic ellipsometry (SE) has been mentioned before.[17] The authors mention that asymmetric PVME concentration values plotted versus diffusion coordinate produce a better fit of their experimental data. The asymmetric PVME concentration profiles should be always expected for diffusion of the liquid polymer in a T_g gradient, as predicted by the model used in our work, and must not always be assigned to a Case II diffusion mechanism. The suggestion of a Case II diffusion mechanism is also supported by an almost-constant diffusion front velocity, as shown in Figure 11 of ref 17; nevertheless, these diffusion experiments were conducted at temperatures located at only 24 K below the glassy matrix T_g and about 100 K above the plasticized-layer T_g. For these experimental conditions, the diffusion in the plasticized layer is conducted along a small T_g gradient, and an almost-constant diffusion front velocity should be expected, as suggested by the simulation results shown in our Figure 11 (where the instantaneous diffusion front velocity is almost constant for the high PS volume fraction zone because the local T_g undergoes minimal changes). The authors make clear that the experimental techniques used do not allow for a direct measurement of PVME concentration versus diffusion coordinate profiles. Therefore, the Fickian tail ahead of the diffusion front mentioned in their work, which was used to improve the fitting of some experimental data, ought to be verified via independent measurements, considering that the authors mention that the fitting is not significantly improved by these Fickian tails. We do not expect any Fickian tails to appear in those experiments, because of the high PVME molecular weight and the corresponding negligible diffusion coefficient values for diffusion of that PVME into the glassy matrix.

Attenuated total reflection Fourier transformed infrared spectroscopy (ATR-FTIR) has also been used to study the interdiffusion between PVME and a glassy PS matrix at temperatures of 15 K below and 5 K above the PS matrix T_g.[19] The authors mention that ATR-FTIR is an indirect technique, in the sense that the measured IR signal represents a summation of contributions from PVME that arrive at different depths from the PVME−PS interface. Furthermore, the depth range from which the IR signal is obtained represents at most 15% of the total original pure PS layer thickness, and this 15% is in contact with the ATR crystal and away from the original PVME−PS interface. The combined facts of measuring the IR signal from the least representative part of the experimental sample and using an integral type of signal make the experimental technique not very accurate or reliable. The experimental data obtained for diffusion at 15 K below the PS T_g have been reported to fit a linear combination of Fickian diffusion with constant diffusion coefficient plus a "Case II model". This fit is taken as evidence for a Case II diffusion mechanism. Also, the experimental data obtained at 5 K *above* the PS-layer T_g is reported to fit a similar linear combination of Fickian diffusion with constant diffusion coefficient plus a Case II model, even though the Case II mechanism has not been defined for diffusion into liquid matrixes. For the above-mentioned reasons, we believe that, for these diffusion experiments, asymmetric PVME concentration versus diffusion coordinate profiles should also be expected. These asymmetric PVME concentration profiles can be fitted with a linear combination of Fickian diffusion with a constant diffusion coefficient, plus a constant-velocity diffusion front displacement, even though the combination does not represent the physical reality of the diffusion process.

For all of the PVME−PS diffusion experiments mentioned above, we expect to find asymmetric PVME concentration versus diffusion coordinate profiles, simply because of the local T_g gradients present along the interphase diffusion path. These asymmetric PVME concentration profiles must not be taken as straightforward evidence for Case II diffusion mechanism, because of the high molecular weight of the PVME used, which is associated with negligible osmotic pressures in contact with a glassy PS matrix, and the extremely low PVME diffusion coefficients in the glassy matrix ahead of the diffusion front. We believe that all of these PVME−PS diffusion experiments can be precisely modeled with the physical diffusion model presented in this work.

The diffusion of liquid PS into a glassy poly(phenylene oxide) (PPO) matrix has been studied using Rutherford backscattering spectrometry (RBS), which is a direct technique, at temperatures between 39 and 6 K below the matrix T_g.[18] Markedly asymmetric PPO concentration versus depth profiles have been measured, with a low slope at low values of the PPO volume fraction and a much greater slope at high values of the PPO volume fraction. These features coincide with our experimental findings and are also predicted by the physical model presented here. Values of the Fickian diffusion coefficient D extracted from the concentration gradients agree with the Kramer model predictions[21−23] (the same scheme used for our calculations) and reveal the importance of considering the influence of the local T_g valueon molecular mobilities.[18] No Fickian tails were reported, which coincides with the results predicted by our calculations.

Conclusions

The experimental results obtained for diffusion of liquid PS into a glassy PPO-rich matrix have been well predicted by a simple physical model for diffusion. The model assumes a relatively rapid dissolution of the high-T_g polymer at the original interface, as suggested by the favorable thermodynamic interaction parameter, and a relatively slow diffusion process that produces a thick interphase. The same physical diffusion model was used previously to predict and correlate results for diffusion of the same polymer pair for diffusion temperatures above the PPO-rich matrix T_g. The agreement obtained for all of these calculations implies that the transport mechanisms are controlled by the diffusion step at the thus-formed interphase.

The diffusion model used for this work predicts, for interdiffusion between polymers pairs with very different T_g values, asymmetric chemical composition profiles for the interphase formed during the diffusion experiments. The shape of these predicted asymmetric profiles were experimentally verified and found to closely resemble some results obtained for the diffusion of small

molecules into glassy matrixes, sometimes defined as Case II diffusion. The model used here does not predict the Fickian tail predicted and observed for Case II diffusion ahead of the moving diffusion front. No experimental evidence for the already-mentioned Fickian tail was observed in this work, in good agreement with the results obtained by other authors.[18,20]

Results obtained from other experiments on the diffusion of liquid polymers into glassy matrixes, published previously by other authors, were also analyzed and compared with our results. It was shown that all of these results can be simply and directly interpreted in terms of the physical diffusion model used here. For all of these experiments, relatively rapid interface dissolution and asymmetric interphase chemical composition profiles are predicted and expected, without any Fickian tail or glassy matrix penetration.

As a general rule, the Case II diffusion mechanism should not be expected for the diffusion of liquid polymers into glassy polymer matrixes, because of the negligible osmotic pressure generated at the glassy interface and the extremely low diffusion coefficients expected for the liquid polymers in the glassy matrixes.

Acknowledgment. Financial support from CONICET through PIP 4384/96 and from CYTED (Iberoamerican Program for the Scientific and Technological Developments) through Project PIP VIII.4 is acknowledged. Also, D.G. acknowledges financial support from CIDAUT.

References and Notes

(1) Vrentras, J. S.; Jarzebski, C. M.; Duda, J. L. *AIChE J*. **1975**, *21* (5), 894.
(2) Thomas, N. L.; Windle, A. H. *Polymer* **1980**, *21*, 613.
(3) Thomas, N. L.; Windle, A. H. *Polymer* **1981**, *22*, 627.
(4) Thomas, N. L.; Windle, A. H. *Polymer* **1982**, *23*, 529.
(5) Durning, C. J. *J. Polym. Sci. B: Polym. Phys.* **1985**, *23*, 1831.
(6) Hui, C.-Y.; Wu, K.-C.; Lasky, R. C.; Kramer, E. J. *J. Appl. Phys* **1987**, *61* (11), 5129.
(7) Hui, C.-Y.; Wu, K.-C.; Lasky, R. C.; Kramer, E. J. *J. Appl. Phys* **1987**, *61* (11), 5137.
(8) Briscoe, B. J.; Pelillo, E.; Ragazzi, F.; Sinha, S. K. *Polymer* **1988**, *39* (11), 2161.
(9) Lasky, R. C.; Kramer, E. J.; Hui, C.-Y. *Polymer* **1988**, *29*, 673.
(10) Gall, T. P.; Lasky, R. C.; Kramer, E. J. *Polymer* **1990**, *31*, 1491.
(11) Kawagoe, M.; Nunomoto, S. *Polymer* **1991**, *32* (17), 3130.
(12) Gall, T. P.; Kramer, E. J. *Polymer* **1991**, *32* (2), 265.
(13) More, A. P.; Donald, A. M.; Henderson, A. *Polymer* **1992**, *33* (17), 3759.
(14) Wu, J. C.; Peppas, N. A. *J. Appl. Polym. Sci.* **1993**, *49*, 1845.
(15) Argon, A. S.; Cohen, R. E.; Patel, A. C. *Polymer* **1999**, *40*, 6991.
(16) Gattiglia, E.; Russell, T. P. *J. Polym. Sci. B: Polym. Phys.* **1989**, *27*, 2131.
(17) Sauer, B. B.; Walsh, D. J. *Macromolecules* **1991**, *24*, 5948.
(18) Composto, R. J.; Kramer, E. J. *J. Mater. Sci.* **1991**, *26*, 2815.
(19) Jabbari, E.; Peppas, N. A. *Macromolecules* **1993**, *26* (9), 2175.
(20) Nealey, P. F.; Cohen, R. E.; Argon, A. S. *Polymer* **1995**, *36* (19), 3687.
(21) Kramer, E. J.; Green, P.; Palmstrom, C. J. *Polymer* **1984**, *25*, 473.
(22) Composto, R. J.; Kramer, E. J.; White, D. M. *Macromolecules* **1988**, *21*, 2580.
(23) Composto, R. J.; Kramer, E. J.; White, D. M. *Polymer* **1990**, *31*, 2320.
(24) Tomba, J. P.; Carella, J. M. *J. Polym. Sci. B: Polym. Phys.* **1999**, *37*, 3097.
(25) Pardo, E.; Tomba, J. P.; Carella, J. M. *Comput. Theor. Polym. Sci.* **2000**, *10* (6), 523.
(26) Tomba, J. P.; Carella, J. M.; Pardo, E. *J. Polym. Sci. B: Polym. Phys.* **1997**, *35*, 2435.
(27) Tomba, J. P.; Carella, J. M.; Pastor, J. M.; Fernández, M. R. *Macromol. Rapid Commun.* **1998**, *19*, 413.
(28) Tomba, J. P.; De la Puente, E.; Pastor, J. M. *J. Polym. Sci. B: Polym. Phys.* **2000**, *38*, 1013.
(29) Tabaksblat, R.; Meier, R. J.; Kip, B. J. *Appl. Spectrosc.* **1992**, *46*, 60.
(30) Tomba J. P.; Elicabe, G. *Appl. Spectrosc.*, manuscript submitted.
(31) Graessley W. W. *Adv. Polym. Sci.* **1982**, *47*, 76.
(32) Ferry, J. D. *Viscoelastic Properties of Polymers*; John Wiley: New York, 1980.
(33) Tomba, J. P.; Carella, J. M.; Pardo, E.; López, S.; Pastor, J. M. *Macromol. Rapid Commun.* **2000**, *21* (14), 983.
(34) Kammer, H.-W.; Inoue, T., Ougizawa, T. *Polymer* **1989**, *30*, 888.
(35) Green, P. F. *Macromolecules* **1991**, *24*, 3373.

MA000529G